BrainZ-BP: A Non-invasive Cuff-less Blood Pressure Estimation Approach Leveraging Brain Bio-impedance and Electrocardiogram

Bufang Yang, Le Liu, and Wenxuan Wu, Mengliang Zhou, Hongxing Liu, Xinbao Ning

Abstract—Accurate and continuous blood pressure (BP) monitoring is essential to the early prevention of cardiovascular diseases. Non-invasive and cuff-less BP estimation algorithm has gained much attention in recent years. Previous studies have demonstrated that brain bio-impedance (BIOZ) is a promising technique for non-invasive intracranial pressure (ICP) monitoring. Clinically, treatment for patients with traumatic brain injuries (TBI) requires monitoring the ICP and BP of patients simultaneously. Estimating BP by brain BIOZ directly can reduce the number of sensors attached to the patients, thus improving their comfort. To address the issues, in this study, we explore the feasibility of leveraging brain BIOZ for BP estimation and propose a novel cuff-less BP estimation approach called BrainZ-BP. Two electrodes are placed on the forehead and occipital bone of the head in the anterior-posterior direction for brain BIOZ measurement. Various features including pulse transit time and morphological features of brain BIOZ are extracted and fed into four regression models for BP estimation. Results show that the mean absolute error, root mean square error, and correlation coefficient of random forest regression model are 2.17 mmHg, 3.91 mmHg, and 0.90 for systolic pressure estimation, and are 1.71 mmHg, 3.02 mmHg, and 0.89 for diastolic pressure estimation. The presented BrainZ-BP can be applied in the brain BIOZ-based ICP monitoring scenario to monitor BP simultaneously.

Index Terms—Brain bio-impedance (BIOZ), Electrocardiogram (ECG), Cuff-less blood pressure (BP) estimation, Pulse transit time (PTT), Machine learning

I. INTRODUCTION

CARDIOVASCULAR diseases (CVDs) have displaced communicable diseases as the major cause of global mortality [1]. Accurate and continuous blood pressure (BP) monitoring is an effective tool to provide early prevention and management of CVDs. Traditional BP measurement usually adopts sphygmomanometer or inflatable cuff-based oscillometer methods, which require applying pressure on the body of subjects by an inflatable cuff [2]. These cuff-based techniques are uncomfortable for users and are not suitable for monitoring circadian fluctuations of BP. Therefore, continuous, non-invasive, and cuff-less BP monitoring techniques have sparked the research community's attention [3]–[5].

Numerous studies demonstrated that pulse wave velocity (PWV) is a prominent indicator to evaluate BP [6]. PWV can be estimated by pulse transit time (PTT), which is the transit time of pulse wave propagation from two different skin sites. Several studies have investigated leveraging PTT for BP estimation, and their experimental results have proved that PTT is useful for BP estimation [7]–[9]. PTT computing

usually requires at least two physiological signals, such as the electrocardiogram (ECG), photoplethysmogram (PPG), and bio-impedance (BIOZ). Leveraging PPG and ECG signals is the most prevalent way for PTT computing [10]–[12]. However, PPG sensors consist of a light source and a photodetector, which is not only affected by environmental light and skin pigmentation but also consumes more power. BIOZ is another non-invasive technique that can be used to compute PTT [13]. Pulsatile change of blood flow in each cardiac cycle causes the variation of BIOZ, thus BIOZ can be used for blood flow and respiration monitoring. BIOZ avoids the shortcoming that PPG is limited by ambient light and power, and has gained a lot of attention in the cuff-less BP monitoring field [14]–[16]. Most existing cuff-less BP estimation approaches leveraging BIOZ signals are based on the wrist BIOZ [14]–[18], ring BIOZ [19] and chest BIOZ [20]. There is currently a scarcity of studies exploring leveraging brain BIOZ for cuff-less BP estimation.

Brain BIOZ is also called rheoencephalography (REG) [21]. It is a valuable non-invasive technique for monitoring intracranial blood flow. The most notable advantage of brain BIOZ lies in its non-invasive nature, allowing for its application in the non-invasive diagnosis of cerebral diseases, including intracranial hemorrhages [22] and traumatic head injuries (TBI) [23]. Brain BIOZ also plays a crucial role in intracranial pressure (ICP) monitoring [24]. ICP measurement is an invasive measurement technique for the human brain, which requires using a probe to measure ICP in the context of craniotomy [25]. As long-term invasive ICP measurement has the risk of intracranial infection, previous studies have begun to explore the utilization of brain BIOZ for non-invasive ICP monitoring [26], [27]. In the intensive care units (ICU), patients with TBI need continuous monitoring of multiple physiological signals, not only ICP but also BP. If BP can be directly estimated by brain BIOZ, the number of sensors attached to the patients can be reduced, thus improving patients' comfort. However, existing research focuses on the utilization of PPG and wrist BIOZ for cuff-less BP estimation [14]–[20], or investigates the correlation between brain BIOZ and ICP [26]–[28]. Studies about the relationship between brain BIOZ and BP are missing, which is the motivation for this study.

To solve these limitations, in this study, we investigate the feasibility of using brain BIOZ for BP estimation for the first time and present a novel cuff-less BP estimation approach called BrainZ-BP. We summarize the contributions of this

paper as follows:

- We implement a novel brain BIOZ-based BP estimation system. To the best of our knowledge, BrainZ-BP is the first work to investigate the feasibility of using brain BIOZ for non-invasive cuff-less BP estimation.
- We develop a novel method for BP estimation based on brain BIOZ that encompasses considerations for signal processing, feature extraction, feature selection, and regression modeling.
- We systematically investigate the effects of important parameters, including excitation frequency and electrode positioning on an individual's head, during brain BIOZ measurement on the accuracy of BP estimation.
- We implement BrainZ-BP and evaluate the performance through extensive experiments on a self-collected brain BIOZ dataset, and open-source the dataset at https://github.com/bf-yang/BrainZ-BP. Results show that BrainZ-BP achieves a mean absolute error of 2.41 mmHg for systolic BP estimation and 2.01 mmHg for diastolic BP estimation, which can effectively applied in the brain BIOZ-based ICP monitoring scenario to monitor BP simultaneously.

II. BACKGROUND AND RELATED WORK

A. Related Works

Brain BIOZ for Health Monitoring. Chen *et al.* [28] investigated the correlation between brain BIOZ and cerebral blood flow (CBF), establishing a mathematical model that serves as a valuable tool for monitoring CBF based on brain BIOZ. In addition, several previous studies have explored the utilization of brain BIOZ for non-invasive ICP monitoring. Bodo *et al.* [26] investigated the correlation between brain BIOZ and ICP for rats. They injected vinpocetine into rats to increase their CBF. After injection, systemic arterial pressure of rats decreases about $25\% \pm 14\%$, and the amplitude of brain BIOZ and ICP signals both increases (BIOZ increase about $209\% \pm 17\%$ and ICP increase about $28\% \pm 16\%$). Traczewski *et al.* [27] studied the correlation between brain BIOZ and ICP obtained from the lumbar puncture. They recruited 62 patients suspected of hydrocephalus in the experiments. Results show that brain BIOZ has clinical value in the diagnosis and prognosis of hydrocephalus.

BIOZ-based BP Estimation. Many studies have been proposed to utilize BIOZ for BP estimation. Ibrahim *et al.* [14] leveraged wrist BIOZ and PPG for cuff-less BP estimation. They employed the AdaBoost regression model for BP estimation based on the extracted PTT, time features, amplitude features, and area features. Their approach achieves a root mean square error (RMSE) of 3.44 mmHg and a mean absolute error (MAE) of 2.51 mmHg for systolic blood pressure (SBP) estimation. For diastolic blood pressure (DBP) estimation, they achieved an RMSE of 2.63 mmHg and an MAE of 1.95 mmHg. Huynh *et al.* [15] also leveraged wrist BIOZ and PPG signals for cuff-less BP estimation. They established the relationship between PTT and BP by employing a quadratic regression model. Their reported RMSE of SBP and DBP are 8.47 mmHg and 5.02 mmHg, respectively. Huynh *et al.*

[16] proposed to only use BIOZ sensors for cuff-less BP estimation. Two BIOZ sensors were placed on the participants' wrists to measure PTT. Subsequently, they utilized the PTT feature, along with the inverse relationship between PTT and PWV, to estimate blood pressure. Wang et al. [17] introduced a continuous BP monitoring system that leverages a single-channel wrist BIOZ signal. They developed a quadratic regression model for accurate BP estimation. The reported MAE for SBP and DBP were 2.01 mmHg and 2.26 mmHg, respectively. Ibrahim et al. [18] employed a wristband BIOZ sensor and a convolutional neural network (CNN) autoencoder for cuff-less BP estimation. Sel et al. [19] developed a ring BIOZ device specifically designed for continuous cuff-less BP estimation, utilizing 15 BIOZ features and an AdaBoost regression model.

In summary, existing research focuses on the utilization of PPG and wrist BIOZ for cuff-less BP estimation, or investigates the correlation between brain BIOZ and ICP. However, studies exploring the feasibility of leveraging brain BIOZ for non-invasive cuff-less BP estimation are currently lacking.

B. Application Scenario and Motivation

Brain BIOZ is also called rheoencephalography (REG) [21]. Blood flow in the brain changes periodically by the cardiac cycle, and the pulsatile change of blood flow causes the variation of BIOZ in the brain: electrical conductivity increases and impedance decreases when blood flows into the brain. Brain BIOZ is a non-invasive technique that enables the monitoring of intracranial blood flow, rendering it valuable for diagnosing cerebral diseases such as intracranial hemorrhages [22] and TBI [23]. In addition, Brain BIOZ also plays a crucial role in ICP monitoring [24]. Continuous and accurate monitoring of ICP is crucial for patients' health as long-term intracranial hypertension can lead to herniation, stroke, and even death. However, traditional ICP measurement is an invasive measurement technique for the human brain, where long-term invasive measurements can result in intracranial infection.

Brain BIOZ allows us to tackle this challenge from a new perspective. Recent studies have shown that brain BIOZ is a promising technique for non-invasive ICP monitoring [26], [27], as it can greatly reduce the risk of intracranial infection. In the ICU, patients with TBI require continuous monitoring of multiple physiological signals, including ICP as well as BP. If BP can be directly estimated using brain BIOZ, it would allow for a reduction in the number of sensors attached to patients, thereby enhancing their comfort. However, existing studies [14]–[18] primarily focus on using wrist BIOZ for BP estimation, and there is a lack of research exploring the relationship between brain BIOZ and BP. This is also the motivation of this study.

C. Principle of BIOZ Measurement

According to the number of electrodes, BIOZ measurement is divided into two types, namely four-electrode and two-electrode setups [29]. Fig. 1 shows the brain BIOZ measurement principle of four-electrode and two-electrode setups.
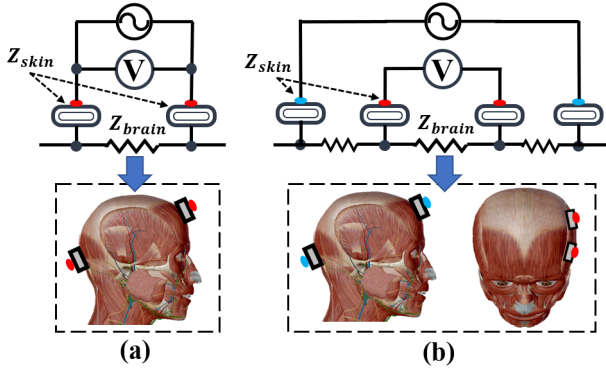
Fig. 1: Principle of four-electrode and two-electrode setups for brain BIOZ measurement. (a) Two-electrode setup, (b) four-electrode setup.

Four-electrode setup uses two separate pairs of electrodes to inject high-frequency injection current and record voltage, respectively. It can obtain accurate impedance values as it avoids the effect of skin-electrode impedance (Z_{skin}) [30]. In the four-electrode setup, the input impedance of the voltage measurement instrument is large enough, i.e. no current flows into the circuit of the voltage measurement instrument, so the effect of Z_{skin} can be ignored. The rationale for four-electrode measurement is shown as follows:

$$V_S = I_c \times Z_{brain} \qquad (1)$$

where I_c is the high-frequency injection current. V_S is the voltage between two measuring electrodes. Z_{brain} is the measured brain BIOZ. Four-electrode setup is suitable for scenarios that require accurate absolute values of BIOZ. Ibrahim $et\ al.$ [14] utilized four-electrode setup for wrist BIOZ measurement. Four electrodes were attached to the radial and ulnar arteries of the wrist. Then they extracted PTT, time, and amplitude features from the wrist BIOZ signal, and used AdaBoost regression model for BP estimation. Wang $et\ al.$ [17] presented a single-channel wrist-BIOZ-based system for BP estimation. Four-electrode setup was used for BIOZ measurement in their study. They used a current pump to provide a continuous excitation current with the frequency of 50 kHz and amplitude of 140 μA.

Two-electrode setup utilizes one pair of electrodes for current injection and voltage measurement simultaneously. The rationale for two-electrode measurement is defined as follows:

$$V_S = I_c \times (Z_{brain} + 2 \times Z_{skin}) \qquad (2)$$

Although the value of measured BIOZ is affected by Z_{skin}, two-electrode measurement can improve users' comfort and reduce the cost and complexity. Therefore, two-electrode technique is suitable for the scenario that requires the impedance variation rather than absolute impedance value [20].

III. MATERIALS AND METHODS

A. System Architecture

Our proposed BrainZ-BP contains a brain BIOZ measurement module and ECG measurement module, which are placed on the head, and the left and right wrists of subjects. Brain BIOZ and ECG signals are recorded by PCI-4474 data acquisition (DAQ) card synchronously. The measured V_S and V_R in the brain BIOZ measurement module are connected to the AI_1 and AI_2 of PCI-4474 DAQ card, respectively. Excitation voltage V_S is provided by signal generator PCI-4461. The output of the ECG module is connected to the AI_3 of PCI-4474 DAQ card. Several data preprocessing methods are utilized to remove the baseline wander and high-frequency noises in the measured brain BIOZ and ECG signals, where the sampling frequency is 100 kHz. Then various features including PTT-based, and morphological features of brain BIOZ are extracted and fed into regression models for SBP and DBP estimation. The prototype of the proposed BrainZ-BP is shown in Fig. 2.

We use a modified two-electrode method for brain BIOZ measurement. A resistor R_0 is connected in series in the circuit. We use a voltage resource V_S and the resistor R_0 to replace the current source. The rationale for brain BIOZ measurement can be written as follows:

$$V_S = V_R + \frac{V_R}{R_0} \times (Z_{brain} + 2 \times Z_{skin}) \qquad (3)$$

$$Z_{brain} \approx \left(\frac{V_S}{V_R} - 1\right) \times R_0 = \left\{ \frac{A_S}{A_R} e^{j(\phi_S - \phi_R)} - 1 \right\} \times R_0 \qquad (4)$$

where V_S is the high-frequency injected voltage. V_R is the voltage of R_0. A_S and A_R are the amplitudes of V_S and V_R, and ϕ_S and ϕ_R are the phases of V_S and V_R, respectively. In this study, V_S is the sinusoidal voltage signal with an amplitude of 1 V_{pp} and frequency of 10 kHz. Numerous studies have shown the safety of applying a voltage signal with a frequency of 10kHz to the human head. R_0 is the 10 kΩ resistor connected in series in the circuit. The equivalent injected current flowing to the subject's head is 0.1 mA. Since the safe voltage and safe current of the human body are 24 V and 10 mA respectively, our circuit parameter settings are safe and reasonable. Two electrodes are placed on the central line of the forehead and occipital bone of the human head in the anterior-posterior direction for Z_{brain} measurement.

ECG signal is recorded by a standard limb lead measurement method (Lead-I). Active electrodes are used in the ECG measurement module. The low output impedance of the active electrode reduces the effect of cable motion artifacts, and thus can improve the measurement performance of biosignal [31].

B. Data Pre-processing

Signal qualities of brain BIOZ and ECG are threatened by four main factors: (1) baseline wandering due to the low-frequency respiration movement and variation of Z_{skin}, (2) power-line interference, (3) high-frequency excitation voltage used for BIOZ measurement, and (4) high-frequency noises caused by body activities and muscular motion.

1) Injection signal filtering: Raw brain BIOZ and ECG contain 10 kHz excitation voltage. N points segmental averaging method is utilized to eliminate this noise interference for ECG. For brain BIOZ, we estimate the amplitude and phase of V_S and V_R for each N points segment, then impedance
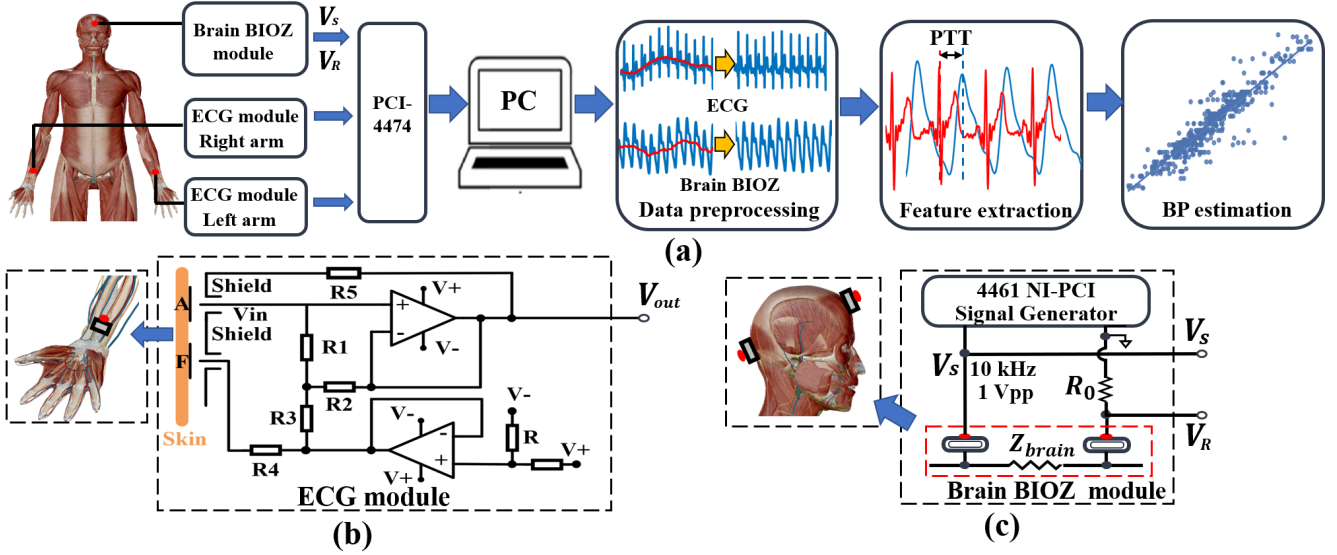
Fig. 2: Prototype of our proposed BrainZ-BP. (a) Overview of the BP estimation system. (b) Schematic of ECG measurement module. (c) Schematic of brain BIOZ measurement module.

can be computed by formula (4). The new sampling rate is $1/N$ of the raw sampling rate. N is set to 200, so the new sampling rates for ECG and brain BIOZ are both 500 Hz. Further, we utilize a 1000-order FIR bandpass filter (0.5-10 Hz) to eliminate power-line interference and high-frequency noises.

2) Baseline calibration: ECG and brain BIOZ contain baseline wandering. Savitzky-Golay (SG) filter is utilized to smooth and denoise the two signals in this study [32]. The advantage of SG filter is that the length and the size of output data can remain the same as the input signal, while noises can be eliminated. In this study, order and window size are set to 3 and 10001 (about 20 seconds), respectively.

3) Segmentation: In this study, a sliding window is utilized to perform data segmentation. Experimental results of previous studies have demonstrated that an 8 seconds window with 6 seconds overlapping is capable to extract key characteristics of cardiac activity [33]. Therefore, 8 seconds sliding window with 75% overlapping is used in this study to split the raw 30-second data into multiple data segments.

Finally, the database contains 1942 ECG and brain BIOZ recordings acquired from 13 subjects. Each 8-seconds recording has two labels (reference SBP and DBP). The mean values of SBP and DBP in the database are 126.3 ± 14.6 mmHg and 73.3 ± 10.2 mmHg, respectively. Fig. 3 shows the statistical distribution of reference SBP and DBP in the database.

C. Feature Extraction

A total of 42 features, including cardiac cycle-based and segment-based features, are extracted from ECG and brain BIOZ in this study. For segment-based features, we calculate them in each 8 seconds data segment. For cardiac cycle-based features, we calculate them in each cardiac cycle and compute the mean as the corresponding features. Fig. 4 shows the schematic diagram of extracted features. The definition of the 42 features used in this study is listed in Table I.
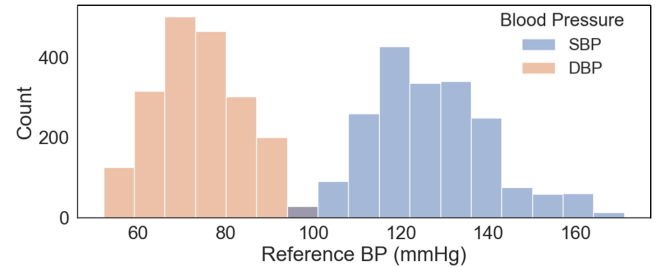

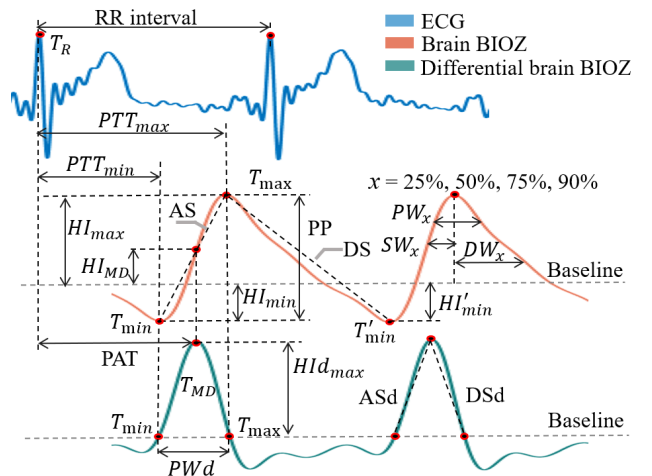Fig. 3: Statistical distribution of SBP and DBP in the database.

Fig. 4: Schematic diagram of PTT-based features, morphological features, height features, slope features and differential signal features.

1) PTT-based features: PTT-based features are considered to be useful in BP estimation [7]–[9]. In this study, three important points in brain BIOZ are utilized to compute PTT features, namely, maximum point, minimum point, and maximum derivative (MD) point. Based on the three points and R

TABLE I: Definition of the extracted features in this study.

No.	Features	Description
1	PTT_{max}	Time delay between R peak of ECG and peak of brain BIOZ
2	PTT_{min}	Time delay between R peak of ECG and minimum point of brain BIOZ
3	PAT	Time delay between R peak of ECG and MD point of brain BIOZ
4	DW	Diastolic width of brain BIOZ
5	DW_{25}	
6	DW_{50}	Diastolic width at x% of the peak of brain BIOZ
7	DW_{75}	x = 25, 50, 75, 90, respectively
8	DW_{90}	
9	SW	Systolic width of brain BIOZ
10	SW_{25}	
11	SW_{50}	Systolic width at x% of the peak of brain BIOZ
12	SW_{75}	x = 25, 50, 75, 90, respectively
13	SW_{90}	
14	PW	Pulse width of brain BIOZ
15	PW_{25}	
16	PW_{50}	Pulse width at x% of the peak of brain BIOZ
17	PW_{75}	x = 25, 50, 75, 90, respectively
18	PW_{90}	
19	PWR_{25}	
20	PWR_{50}	
21	PWR_{75}	Ratio of pulse width at x% of the peak to total pulse width
22	PWR_{90}	
23	HI_{max}	Maximum height of brain BIOZ
24	HI_{min}	Minimum height of brain BIOZ
25	HI_{MD}	MD point height of brain BIOZ
26	PP	Height difference between HI_{max} and HI_{min}
27	HIR_{max}	Ratio of HI_{max} and HI_{min}
28	HIR_{MD}	Ratio of HI_{MD} and HI_{min}
29	AS	Ascending slope of brain BIOZ
30	DS	Descending slope of brain BIOZ
31	HId_{max}	Maximum height of differential brain BIOZ
32	PWd	Pulse width of differential brain BIOZ
33	PWd_{50}	Pulse width at 50% of the peak of differential brain BIOZ
34	PWRd	Ratio of PWd_{50} to PWd
35	ASd	Ascending slope of differential brain BIOZ
36	Dsd	Descending slope of differential brain BIOZ
37	SD	Standard deviation of brain BIOZ
38	Skew	Skewness of brain BIOZ
39	Kurt	Kurtosis of brain BIOZ
40	ApEn	Approximate entropy of brain BIOZ
41	SampEn	Sample entropy of brain BIOZ
42	HR	Heart rate

peak of ECG, PTT_{max}, PTT_{min}, and PAT are calculated in each cardiac cycle, which are defined as follows:

$$PTT_{max} = T_{max} - T_R \tag{5}$$

$$PTT_{min} = T_{min} - T_R \tag{6}$$

$$PAT = T_{MD} - T_R \tag{7}$$

where T_{max}, T_{min}, T_{MD} and T_R are the time of maximum point, minimum point, MD point of brain BIOZ, and of the R peak of ECG in the current cardiac cycle, respectively.

2) Morphological features: Morphological features of brain BIOZ can reflect the cardiovascular condition, which is crucial for BP estimation [14]. Morphological features consist of pulse width (PW), systolic width (SW), and diastolic width (DW) of brain BIOZ, which are defined as follows:

$$PW = T'_{min} - T_{min} \tag{8}$$

$$SW = T_{max} - T_{min} \tag{9}$$

$$DW = T'_{min} - T_{max} \tag{10}$$

where T'_{min} is the minimum point of brain BIOZ in the next cardiac cycle. PW, SW, and DW at 25%, 50%, 75%, and 90% of the peak of brain BIOZ are extracted in each cardiac cycle, which are denoted as PWx, SWx, and DWx, respectively. Further, the ratio of PWx and the total width PW are calculated, which is denoted as PWRx.

3) Height features: Height features of brain BIOZ, including maximum height (HI_{max}), minimum height (HI_{min}), MD point height (HI_{MD}), and peak to peak (PP) value are extracted for each cardiac cycle. Further, height ratio features HIR_{max} and HIR_{MD} are extracted, which are defined as:

$$HIR_{max} = \frac{HI_{max}}{HI_{min}} \tag{11}$$

$$HIR_{MD} = \frac{HI_{MD}}{HI_{min}} \tag{12}$$

4) Slope features: Slope features are considered to be useful for BP estimation since they can reflect the velocity of CBF. Two slope features are computed in this work, namely, ascending slope (AS) and descending slope (DS). AS and DS represent the slope in the systolic area and diastolic area, respectively, which are defined as follows:

$$AS = \frac{HI_{max} - HI_{min}}{T_{max} - T_{min}} \tag{13}$$

$$DS = \frac{HI_{max} - HI'_{min}}{T_{max} - T'_{min}} \tag{14}$$

5) Statistical features: In this study, three statistical features including standard deviation (SD), skewness (Skew), and kurtosis (Kurt) are extracted for each 8-s brain BIOZ segment.

6) Entropy features: Entropy features are useful quantization indicators for complexity and irregularity of time series [34]. Approximate entropy (ApEn) and sample entropy (SampEn) of brain BIOZ are extracted in this study.

7) Differential signal features: First-order difference of brain BIOZ is an effective quantization indicator for the velocity of blood flow in the human brain. Maximum height (HId_{max}), pulse width (PWd), pulse width at 50% height of the peak (PWd_{50}), and the ratio of PWd_{50} and PWd are calculated in each cardiac cycle. We also extracted the ascending slope (ASd) and descending slope (DSd) features, which can reflect the acceleration of CBF.

PTT-based features, morphological features, height features, slope features, and differential signal features are cardiac cycle-based features, while statistical features and entropy features are segment-based features.

D. Feature Importance Analysis

Hand-crafted features may contain redundant information. To gain a deeper understanding of the importance of hand-crafted features in BP estimation, we consider two types of feature importance analysis techniques feature importance evaluation, namely Pearson correlation coefficient (PCC) and random forest impurity. PCC and random forest impurity are linear and non-linear techniques for feature importance evaluation. However, whether to employ either of these methods individually or combine them for feature selection, leading to a more accurate BP estimation, is still an open problem. In this study, we compare three approaches for feature selection, namely PCC, random forest impurity, and their combination.

1) Pearson correlation coefficient: PCC is an effective technique for feature importance analysis, which can reflect the linear correlation between each feature and the corresponding predicted value [35]. PCC is defined as follows:

$$r_{xy} = \frac{\sum_{i=1}^{N} \{(x_i - \mu_x) \cdot (y_i - \mu_y)\}}{\sqrt{\sum_{i=1}^{N}(x_i - \mu_x)^2} \cdot \sqrt{\sum_{i=1}^{N}(y_i - \mu_y)^2}} \quad (15)$$

where x_i and y_i are the extracted feature variable and the BP value of the i-th sample, respectively. μ_x and μ_y are the mean of the feature and the mean of the BP value in N data samples. r_{xy} is between -1 and 1. A closer absolute value of r_{xy} to 1 means a higher linear correlation. According to the $abs(r_{xy})$ of each feature, PCC importance ranking is obtained (larger absolute r_{xy} ranks higher).

2) Random forest impurity: We also utilize a non-linear feature importance evaluation method called random forest impurity [4]. Random forest impurity method uses the impurity of each feature to evaluate the feature importance during tree model recursively building, which is an embedded feature selection method [36].

Random forest (RF) is an ensemble tree model, which integrates multiple Classification and Regression Trees (CART) [37]. The construction process of each CART is essentially a process of feature selection. The objective function of each CART is as follows:

$$Obj = \min_{j,s} \left\{ \min_{c_1} \sum_{x_i \in R_1} (y_i - c_1)^2 + \min_{c_2} \sum_{x_i \in R_2} (y_i - c_2)^2 \right\} \quad (16)$$

Based on the j-th feature and feature splitting point s, data is split into two partitions, namely R_1 and R_2. For each partition R, the predicted value is denoted as $c = \frac{1}{n} \sum_{i \in R} y_i$. Mean square error (MSE) is used as loss function to find the optimal splitting feature and splitting point. Suppose N is the total number of samples, M is the total times of X used as the splitting feature in CART, the importance of feature X is defined as:

$$I_C(X) = \sum_{i=1}^{M} \left\{ P\left(R^{(i)}\right) N_R^{(i)} - P\left(R_l^{(i)}\right) N_{R_l}^{(i)} - P\left(R_r^{(i)}\right) N_{R_r}^{(i)} \right\} \quad (17)$$

where $R^{(i)}$ is the partition before the i-th splitting using feature X. $R_l^{(i)}$ and $R_r^{(i)}$ are the left and right partitions after the i-th splitting. $N_R^{(i)}$, $N_{R_l}^{(i)}$ and $N_{R_r}^{(i)}$ are the number of samples of partitions $R^{(i)}$, $R_l^{(i)}$ and $R_r^{(i)}$, respectively. $P(\cdot)$ represents the impurity of the partition, i.e. MSE value.

Let D be the number of CART in RF, the importance of feature X in the random forest is defined as:

$$I_{RF}(X) = \frac{1}{D} \sum_{i}^{D} I_i(X) \quad (18)$$

where $I_i(X)$ is the importance of feature X in the i-th CART.

3) Combining two methods for feature selection: To evaluate the linear and non-linear correlation between each feature and BP value simultaneously, we first use PCC and RF impurity methods respectively to calculate their respective feature importance ranking. Then, the average of two rankings

is used as the feature importance score. According to the importance score, the final ranking is obtained.

E. Regression Models

Numerous machine learning (ML) algorithms have been proposed and widely employed for health monitoring systems [38]–[40]. In this work, four ML models are used for BP estimation, including linear regression (LR), support vector machine (SVM), decision tree (DT), and random forest (RF). Details about these models are as follows:

1) Linear regression: LR is a frequently used regression model, which builds the linear relationship between the input feature vector and the predicted variable. It is regarded as a baseline model in our experiment.

2) Support vector machine: SVM is a powerful statistical machine learning algorithm, which is also called SVR when it is applied in regression task [41]. The training strategy of SVR model is based on the structural risk minimization principle. SVR maps the data from low-dimension space into high dimension space and searches for an optimal hyperplane. It is suitable for small-sample learning problems.

3) Decision tree and Random forest: The advantage of DT lies in its high interpretability and low computational cost [42]. RF is an ensemble model, integrating multiple decision trees, which belongs to bagging ensemble learning. It utilizes bootstrap sampling, introducing sample variation and feature variation, thereby reducing the variance of the base model. Suppose there are D CARTs in the RF model, and the output of RF can be expressed as follows:

$$RF(x) = \frac{1}{D} \sum_{i=1}^{D} CART_i(x) \quad (19)$$

where $CART_i(x)$ is the predicted value of the i-th CART.

F. Experimental Protocol

The experiment was conducted under the IRB approval (2022DZKY-040-01) by Nanjing Jinling Hospital. A total of 13 healthy subjects without any history of cardiovascular diseases were recruited for our experiment (11 males, 2 females, age: 23.6 ± 1.6 years, height: 171.5 ± 6.7 cm, weight: 65.3 ± 12.6 kg). The mean body mass index (BMI) of these subjects are 22.0 ± 2.9 kg/m^2.

A total of 10 measurement trials are conducted for each subject. Each trial lasts for 30 seconds. During each trial, ECG, brain BIOZ, reference SBP, and DBP, are recorded synchronously for each subject. Fig. 5 shows the experimental scenario. During data measurement, participants are required to sit quietly and remain still to avoid signal noises and motion artifacts. Reference SBP and DBP values are recorded by a cuff-based BP device (BSX-533, Haier, China), which is placed on the right upper arm.

Since BP will not change largely if subjects just sit on the seat quietly. To obtain a wider range of BP values, subjects are required to conduct physical exercises in the experiment. Before the fifth measurement trial started, subjects were required to conduct high knee exercises for 2 minutes.
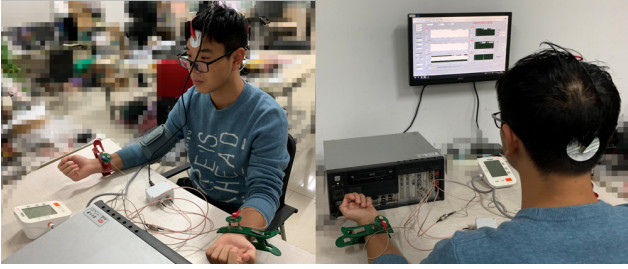
Fig. 5: Experimental scenario.

Fig. 6: The processed brain BIOZ signal.

After high knee exercise, the BP value of each subject will increase largely, where SBP will increase about 10-30 mmHg, and DBP will increase about 5-10 mmHg. We also try to instruct subjects to conduct other exercises such as the squat, but it is harmful to their knees, and is difficult to increase DBP value via this exercise. After high knees exercise, subjects are required to remain still again during the sixth to tenth measurement trials. The BP value of subjects will gradually decrease until it returns to its normal level. In this way, the BP value of subjects will first increase and then decrease during the 10 trials, so a wider range of BP values are recorded.

G. Model Development and Performance Evaluation

A total of 1942 recordings from 13 subjects were collected in our experiments. We perform 10-fold cross-validation to evaluate the BP estimation performance of our method. In this study, RF contains 500 decision trees, and the minimum number of samples in the leaf node is 1. We also experimented with the number of trees ranging from 10 to 1000. Results show that the estimation performance improves obviously when the tree number increases from 10 to 500, but the performance can hardly improve when the tree number is larger than 500. Therefore, the tree number is set to 500 in our experiment. Radial basis function (RBF) kernel is used for SVR model, and the regularization parameter is set to 10^3 in our experiments.

Mean error (ME), mean absolute error (MAE), root mean square error (RMSE), and correlation coefficient (R) are used to evaluate the BP estimation performance in this study. ME and RMSE are utilized to assess whether the BP estimation model satisfies the Association for the Advancement of Medical (AAMI). MAE is used to assess the BP estimation model in accordance with the British Hypertension Society (BHS) standard.

IV. Experiments and Results

A. Brain BIOZ Waveforms

Fig. 6 shows the example of measured brain BIOZ when two electrodes are placed on the forehead and occipital bone of the head in an anterior-posterior direction. From top to bottom are the real part, imagine part, and the absolute value of the brain BIOZ signal. As can be seen, the absolute value of brain BIOZ has the highest amplitude (about 32 Ω), followed by the image part and the real part (about 23 Ω and about 13 Ω, respectively). The phenomenon that the absolute value of
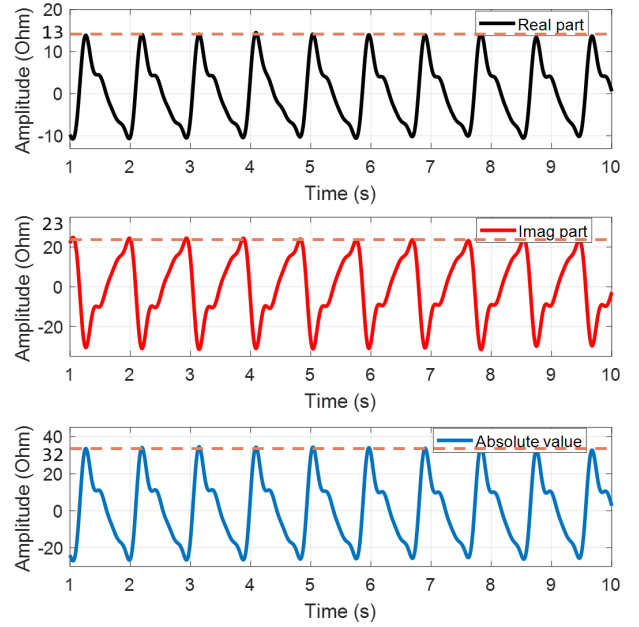
brain BIOZ provides the largest impedance change also occurs in other data segments. A larger amplitude of brain BIOZ can better reflect CBF change. Therefore, the absolute value of brain BIOZ is used for analysis in this study.

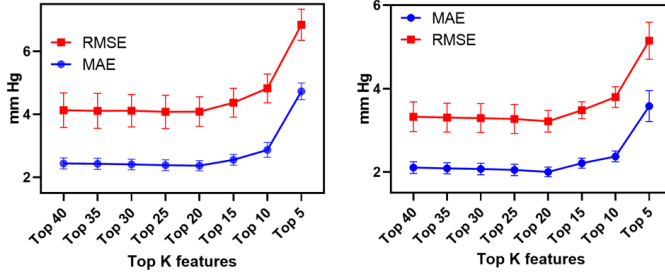#### B. Feature Importance Analysis

Fig. 7 shows the BP estimation performance using three types of methods to select the top K important features. For each K, a 10-fold cross-validation experiment is conducted. It is observed that the estimated error of PCC and random forest impurity both exhibit a trend of initially decreasing and then increasing as the number of top K features used is reduced (Fig. 7a and Fig. 7b). This can be attributed to the fact that irrelevant and redundant features can be harmful to machine learning algorithms [43], [44], i.e. increasing the prediction error and training speed. Furthermore, random forest impurity exhibits a more pronounced trend of decreasing and then increasing compared to PCC. It also achieves a lower estimation error for both SBP and DBP at its optimal point. However, when employing the feature selection method that combines PCC and random forest impurity (as introduced in Section III-D), it demonstrates an almost monotonic increasing trend. The optimal point is reached when utilizing the top 25 important features, but the estimated error is higher compared to using random forest impurity alone for feature selection.

For ease of comparison, we have summarized the best results from each approach in Table II. We can see that using random forest impurity for feature selection achieves the lowest BP estimation error and requires the fewest number of features. While integrating PCC and random forest impurity provides a comprehensive perspective on feature importance (linear and non-linear relationships), combining the two approaches does not yield better results and even leads to worse performance. Therefore, we opt for random forest

TABLE II: The best result of each approach and the number of features they used (K value).

|	Evaluation Metrics	PCC	Random forest impurity	Combi-nation
SBP	RMSE (mmHg)	4.08 ± 0.44	$\mathbf{3.91 \pm 0.53}$	4.14 ± 0.61
	MAE (mmHg)	2.37 ± 0.15	$\mathbf{2.17 \pm 0.18}$	2.38 ± 0.22
DBP	RMSE (mmHg)	3.21 ± 0.24	$\mathbf{3.02 \pm 0.46}$	3.54 ± 0.46
	MAE (mmHg)	2.00 ± 0.11	$\mathbf{1.71 \pm 0.18}$	2.19 ± 0.14
	Number of features	20	**10**	25

impurity as the feature importance ranking strategy in BrainZ-BP, as it demonstrates superior performance and efficiency in feature selection. Based on the results in Fig. 7b, the top 10 important features selected by random forest impurity are used in BrainZ-BP.

(a) PCC. The left and right figures are SBP and DBP estimations, respectively.
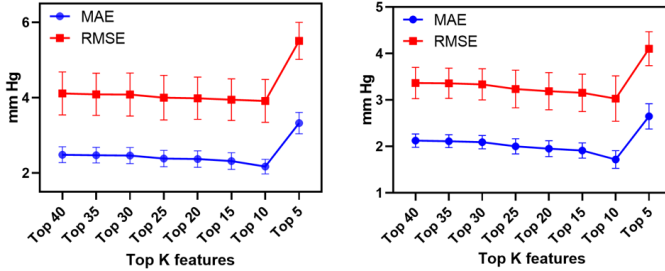
(b) Random forest impurity. The left and right figures are SBP and DBP estimations, respectively.
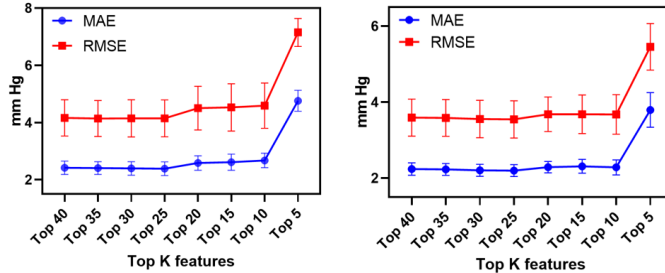
(c) Combination of PCC and random forest impurity. The left and right figures are SBP and DBP estimations, respectively.

Fig. 7: BP estimation performance using three types of methods to select the top K important features. (a) and (b) are from PCC. (c) and (d) are from random forest impurity. (e) and (f) are from the combination of PCC and random forest impurity.

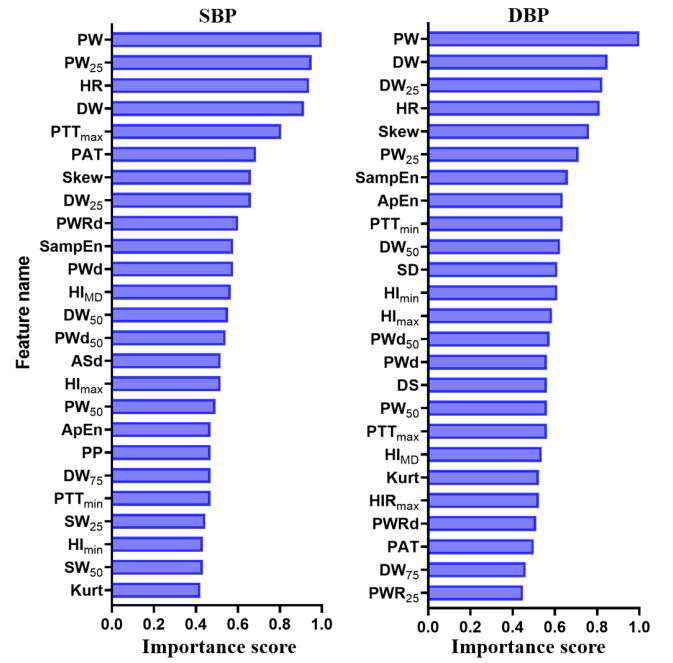Feature importance ranking for SBP and DBP estimation are

Fig. 8: Feature importance ranking for SBP and DBP estimation.

shown in Fig. 8 (only the top 25 most important features are listed). As can be seen, morphological features of brain BIOZ, e.g. PW, PW_{25}, DW, DW_{25}, play a crucial role both in SBP and DBP estimation, which is consistent with study [2]. The pulse width of brain BIOZ (PW) has the highest importance score both for SBP and DBP estimation. Additionally, PTT-based features including PTT_{max}, PTT_{min}, PAT, are also important for both SBP and DBP estimation, as previously shown in studies [7]–[10].

C. Performance of BP Estimation

Fig. 9 shows the histograms of SBP and DBP estimation errors using RF. As can be seen from the histograms, most of the predicted errors are distributed around zero, within the range of $\pm$ 20 mmHg, which is similar to the Gaussian distribution with zero means. Fig. 10 presents the correlation plots of estimated BP with reference BP using RF. Correlation coefficient R is 0.90 and 0.89 for SBP and DBP estimation, which illustrates the estimated BP of our method is highly correlated with reference BP. Fig. 11 shows the Bland-Altman plots of SBP and DBP estimation. X-axis and Y-axis are the mean and error of reference BP and estimated BP respectively. Bland-Altman plots illustrate that most of the predicted errors of SBP and DBP are within 0.39 ± 8.92 mmHg and -0.07 ± 6.97 mmHg limits. Therefore, our proposed approach is an effective BP estimation method.

Additionally, we compare the BP estimation performance of the four regression models, as shown in Table III. As can be seen, the estimation performance of LR model is obviously lower than the other three regression models. R is only 0.41 and 0.30 for SBP and DBP estimation, respectively. Amongst the other three regression models, RF achieves the best BP estimation performance. The RMSE of RF is 3.91 and 3.02
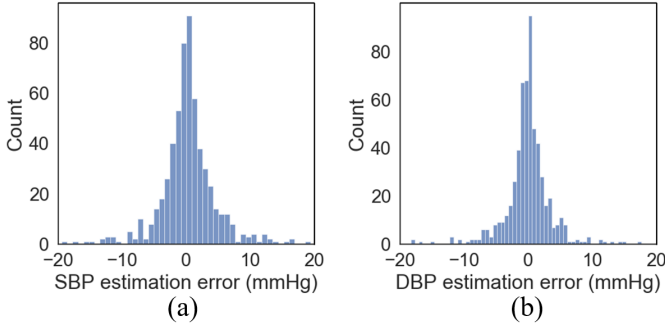
Fig. 9: Histograms of estimation error using RF model. (a) SBP estimation. (b) DBP estimation.
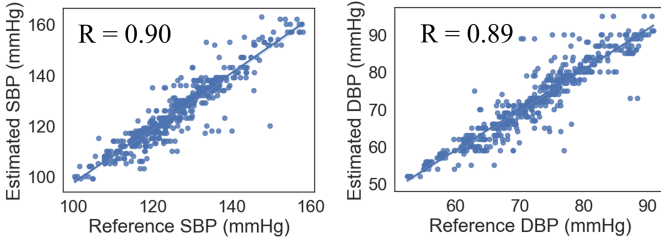

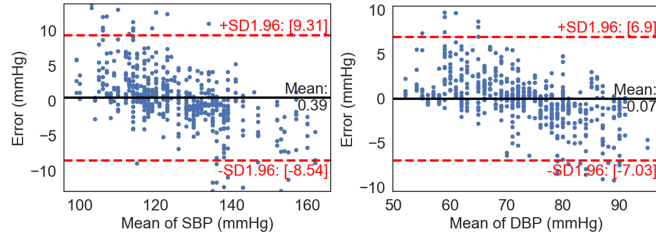Fig. 10: Correlation plots of estimated BP with reference BP.

Fig. 11: Bland-Altman plots of SBP and DBP estimation.

TABLE III: BP estimation performance of different regression models.

Models	Evaluation metrics	SBP	DBP
LR	MAE (mmHg)	8.14 ± 0.38	6.61 ± 0.33
	RMSE (mmHg)	10.40 ± 0.56	8.28 ± 0.37
	R	0.41 ± 0.06	0.30 ± 0.03
SVR	MAE (mmHg)	3.11 ± 0.31	2.59 ± 0.26
	RMSE (mmHg)	5.58 ± 0.85	4.45 ± 0.56
	R	0.82 ± 0.05	0.79 ± 0.04
DT	MAE (mmHg)	2.20 ± 0.40	2.02 ± 0.24
	RMSE (mmHg)	6.04 ± 1.14	5.07 ± 0.46
	R	0.79 ± 0.07	0.73 ± 0.04
RF	MAE (mmHg)	2.17 ± 0.18	1.71 ± 0.18
	RMSE (mmHg)	3.91 ± 0.53	3.02 ± 0.46
	R	0.90 ± 0.02	0.89 ± 0.02

TABLE IV: Comparison of our method with AAMI standards.

	SBP		DBP	
	Results	AAMI	Results	AAMI
ME (mmHg)	0.08	≤ 5	0.01	≤ 5
RMSE (mmHg)	4.11	≤ 8	3.36	≤ 8

TABLE V: Comparison of our method with BHS standards.

		Cumulative Error Percentage (CP)		
		$\leq$5mmHg	$\leq$10mmHg	$\leq$15mmHg
Results	SBP	83.1%	95.0%	98.6%
	DBP	86.9%	97.7%	99.1%
BHS standards	Grade A	$\geq 60\%$	$\geq 85.0\%$	$\geq 95\%$
	Grade B	$\geq 50\%$	$\geq 75.0\%$	$\geq 90\%$
	Grade C	$\geq 40\%$	$\geq 65.0\%$	$\geq 85\%$

mmHg for SBP and DBP estimation, MAE is 2.17 and 1.71 mmHg, and R is 0.90 and 0.89, respectively.

Table IV and Table V show the comparison of our methods (using RF model) with AAMI and BHS standards. The ME and RMSE of our proposed method are less than 5 and 8 mmHg, respectively (both the SBP and DBP satisfy), which suggests our method passes the AAMI standard. Further, for SBP estimation, CP ($\leq$ 5 mmHg) is 82.8%, CP ($\leq$ 10 mmHg) is 94.3% and CP ($\leq$ 15 mmHg) is 98.2%, respectively. For DBP estimation, CP ($\leq$ 5 mmHg) is 87.9%, CP ($\leq$ 10 mmHg) is 97.2% and CP ($\leq$ 15 mmHg) is 99.1%, respectively. Results suggest the performance of our method achieves the A level of BHS standard both for SBP and DBP estimation.

V. DISCUSSION

A. Comparison with Previous Studies

In this paper, we investigate the feasibility of using brain BIOZ for BP estimation and present BrainZ-BP. Table VI illustrates the comparison of our proposed method with other existing studies using BIOZ for BP estimation. Ibrahim et al. [14] placed BIOZ sensor and PPG on the wrist of participants. They extracted a total of fifty features, including PTT, time features, amplitude features, and area features. Subsequently, they

employed AdaBoost regression model for BP estimation. Ten healthy subjects, aged between 18 and 30 years, were recruited for the experiments. Their method achieved RMSE and MAE of 3.44 and 2.51 mmHg for SBP estimation, and achieved 2.63 and 1.95 mmHg for DBP estimation, respectively. Huynh et al. [15] extracted PTT features from wrist BIOZ and PPG signals. The relationship between PTT and BP was determined by employing a quadratic regression model. Fifteen healthy subjects, with an average age of 29 years, were recruited for the study. Their reported RMSE of SBP and DBP are 8.47 $\pm$ 0.91 mmHg and 5.02 $\pm$ 0.73 mmHg, respectively. Huynh et al. [16] also proposed to position two BIOZ sensors on the wrists of participants to measure PTT. They then utilized the PTT feature, along with the inverse relationship between PTT and PWV, to estimate BP. Wang et al. [17] proposed a continuous BP monitoring system leveraging single-channel wrist BIOZ, and they also build a quadratic regression model for BP estimation. Thirty subjects, with an average age of 27 years, participated in the experiments. Their reported MAE are 2.01 $\pm$ 1.40 mmHg and 2.26 $\pm$ 1.43 mmHg for SBP and DBP, respectively. Ibrahim et al. [18] utilized a wristband BIOZ sensor and employed a CNN autoencoder for BP estimation.

In the experiments conducted on a sample of four subjects aged between 20 and 25 years, they achieved a RMSE of 6.5 mmHg for SBP estimation and a RMSE of 5.0 mmHg for DBP estimation. Sel et al. [19] developed a ring-BIOZ-based cuff-less BP estimation device, utilizing 15 BIOZ features and an AdaBoost regression model. They recruited 10 health subjects in their mid-twenties for experiments and achieved an RMSE of 5.27 mmHg for SBP estimation and 3.87 mmHg for DBP estimation.

We can see that our proposed method achieves higher estimation performance than studies [15], [16], and achieves similar performance as studies [14], [17]. The RMSE and R of the proposed method surpass the method in [15] with an improvement of 4.41 mmHg and 0.02 for SBP estimation, and of 1.77 mmHg and 0.01 for DBP estimation, respectively. Further, the RMSE and R of our method outperform the method in [16] with an improvement of 3.41 mmHg and 0.09 for SBP, and of 1.92 mmHg and 0.05 for DBP, respectively. Since all the aforementioned studies adopted the subject-dependent paradigm to conduct experiments, the comparison in this study is fair. Results show that brain BIOZ is a promising technique for BP estimation.

B. Effect of Excitation Frequency

We carry out an additional experiment to investigate the influence of excitation frequency on brain BIOZ measurement. Excitation frequency changes from 1 kHz to 20 kHz. The difference between the maximum and minimum of brain BIOZ in each cardiac cycle is denoted as ΔZ. ΔZ and SampEn are used as indicators to evaluate the performance of brain BIOZ measurement in this study. Larger ΔZ can better reflect the CBF change. SampEn can reflect the irregularity of time series. A lower SampEn value means the higher signal quality of the measured brain BIOZ.

Fig. 12 shows the waveform of brain BIOZ from different excitation frequencies. It can be seen that lower excitation frequency has larger ΔZ, e.g. ΔZ is 31.3 Ω and 55.2 Ω when excitation frequencies are 20 kHz and 10 kHz, respectively. However, when excitation frequency decreases to 2 kHz, the waveform of brain BIOZ contains obvious fluctuation. When excitation frequency decreases to 1 kHz, the waveform of BIOZ has poor regularity due to the great effect of skin-electrode impedance. We utilize data in 100 cardiac cycles to calculate the mean and SD of SampEn and ΔZ, as shown in Fig. 13. As can be seen, ΔZ increases as excitation frequency decreases. However, when excitation frequency decreases to 2 kHz, SampEn of brain BIOZ increases largely. The mean SampEn is 0.060 and 0.058 for 1 kHz and 2 kHz, respectively, while the mean SampEn is only about 0.045 for 5 - 20 kHz, where 10 kHz excitation frequency has the best signal quality with 0.043 mean SampEn.

Results demonstrate that lower excitation frequency has a larger ΔZ. However, too low excitation frequency will bring larger skin-electrode impedance, which may lead to low signal quality of the measured brain BIOZ. 10 kHz excitation frequency is able to produce relatively large ΔZ, and is less affected by skin-electrode impedance. Therefore, 10 kHz excitation frequency is used in this study.
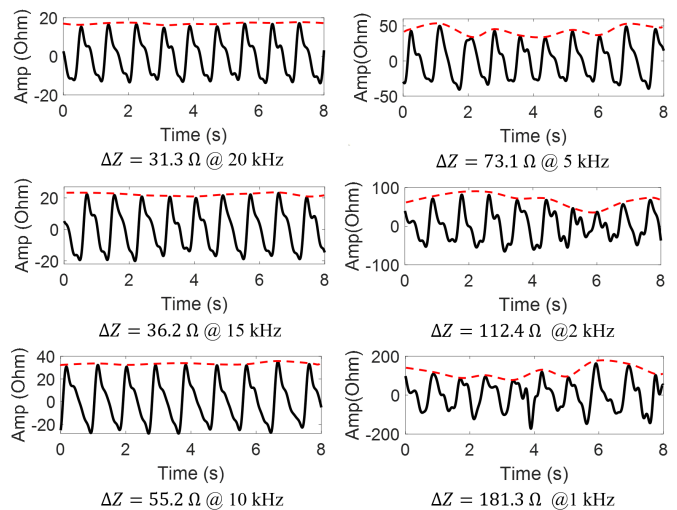

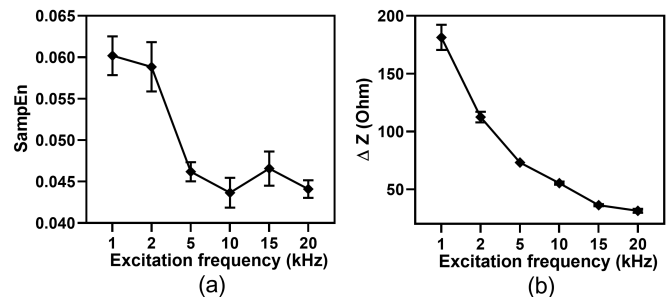Fig. 12: Brain BIOZ waveform from different excitation frequency.

Fig. 13: SampEn and ΔZ of brain BIOZ from different excitation frequency. (a) SampEn. (b) ΔZ.

C. Effect of Electrode Position

Electrode position plays an essential role in BIOZ measurement [15], [17]. Therefore, we investigate the effect of electrodes placed in the anterior-posterior direction and in the left-right direction on brain BIOZ measurement. For anterior-posterior direction placement, two electrodes are placed on the forehead and the occipital bone of the human head, respectively. For left-right direction placement, two electrodes are placed on the left and right temple, respectively. As can be seen from Table VII, anterior-posterior direction placement of electrodes can provide larger ΔZ than left-right direction under the excitation frequency of 2 kHz to 20 kHz. For 10 kHz excitation frequency, anterior-posterior direction and left-right direction have almost the same SD of ΔZ (3.96 Ω for anterior-posterior, and 3.97 Ω for left-right direction), but anterior-posterior direction can obtain larger mean of ΔZ (55.27 Ω for anterior-posterior direction, and 37.35 Ω for left-right direction). Therefore, two electrodes are placed on the forehead and occipital bone of the human head in this study.

D. Limitations and Future Works

However, there are some limitations of this work. In this pioneering study, we recruited 13 young subjects without any history of cardiovascular diseases to participate in the

TABLE VI: Comparison of our proposed method with existing studies using BIOZ for BP estimation.

Studies	Subjects	Signals	Models	SBP			DBP		
				MAE	RMSE	R	MAE	RMSE	R
Ref. [14]	10	Wrist BIOZ + PPG	AdaBoost	2.51	3.44	0.86	1.95	2.63	0.77
Ref. [15]	15	Wrist BIOZ + PPG	Quadratic Regression	-	8.47	0.88	-	5.02	0.88
Ref. [16]	15	Wrist BIOZ	PWV model	-	7.47	0.81	-	5.17	0.84
Ref. [17]	30	Wrist BIOZ	Quadratic Regression	2.01	-	0.95	2.26	-	0.75
Ref. [18]	4	Wrist BIOZ	CNN autoencoder	-	6.5	0.79	-	5.0	0.80
Ref. [19]	10	Ring BIOZ	AdaBoost	-	5.27	0.76	-	3.87	0.81
This work	13	Brain BIOZ + ECG	RF	2.17	3.91	0.90	1.71	3.02	0.89

TABLE VII: Mean $\pm$ SD of ΔZ using anterior-posterior and left-right direction electrodes placement.

Electrodes placement	Index	2 kHz	5 kHz	10 kHz	15 kHz	20 kHz
Anterior-posterior	Mean	112.49	73.14	55.27	36.27	31.38
	SD	10.84	6.14	3.96	2.51	3.37
Left-right	Mean	71.06	49.38	37.35	26.63	23.76
	SD	7.18	4.95	3.97	1.81	2.55

experiments. Like many existing studies on BIOZ-based BP estimation [14]–[17], we also adopted the subject-dependent paradigm for our experiments. It means BrainZ-BP is a personalized model that requires a calibration process in practical application for each user, i.e. it requires collecting data for each user in advance for model training before the model works, no matter in the case of individuals with health conditions or advanced age. In the future, we plan to recruit a larger number of subjects encompassing a broader range of ages and clinical conditions to perform the subject-independent experiment and enhance the generalizability of BrainZ-BP. Secondly, in this pilot study, we only collected BP data from subjects. In future work, we plan to perform experiments to collect the BP and ICP data simultaneously and study a regression model that leverages brain BIOZ to estimate BP and ICP simultaneously. Finally, recent studies have introduced the utilization of magnetic sensors, such as magnetocardiography, for the contactless monitoring of BIOZ [45] and cardiac signal [46]. BrainZ-BP monitoring system can also expand to using magnetic sensors for contactless BP estimation. We leave this as our future work.

VI. CONCLUSION

In this paper, we explore the feasibility of using brain BIOZ for BP estimation and present a novel cuff-less BP estimation model called BrainZ-BP. BrainZ-BP utilizes brain BIOZ and ECG signals for BP estimation. Various features including PTT-based and morphological features of brain BIOZ are extracted. We use the Pearson correlation coefficient and random forest impurity methods to select the top 25 important features. The selected features are fed into the random forest regression model for BP estimation. Results show that the MAE, RMSE, and R of BrainZ-BP are 2.17 mmHg, 3.91 mmHg, and 0.90 for SBP estimation, and are 1.71 mmHg, 3.02 mmHg, and 0.89 for DBP estimation. The proposed BrainZ-BP both satisfies AAMI and BHS standards. Results show

that brain BIOZ is a promising technique for BP estimation. The presented BrainZ-BP model can be applied in the brain BIOZ-based non-invasive ICP monitoring scenario to monitor BP simultaneously.

REFERENCES

[1] W. H. Organization, "A global brief on hypertension : silent killer, global public health crisis: World health day 2013," technical documents, 2013.

[2] D. Wang, "Photoplethysmography-based blood pressure estimation combining filter-wrapper collaborated feature selection with LASSO-LSTM model," *IEEE Trans. Instrum. Meas.*, vol. 70, pp. 1–14, 2021.

[3] X. He, R. A. Goubran, and X. P. Liu, "Secondary peak detection of PPG signal for continuous cuffless arterial blood pressure measurement," *IEEE Trans. Instrum. Meas.*, vol. 63, no. 6, pp. 1431–1439, 2014.

[4] S. Yang, J. Sohn, S. Lee, J. Lee, and H. C. Kim, "Estimation and validation of arterial blood pressure using photoplethysmogram morphology features in conjunction with pulse arrival time in large open databases," *IEEE J. Biomed. Health Inform.*, vol. 25, no. 4, pp. 1018–1030, 2021.

[5] P. C.-P. Chao, C.-C. Wu, and D. H. Nguyen, "The machine learnings leading the cuffless PPG blood pressure sensors into the next stage," *IEEE Sensors J.*, vol. 21, no. 11, pp. 12498–12510, 2021.

[6] V. Chandrasekaran, R. Dantu, S. Jonnada, and S. Thiyagaraja, "Cuffless differential blood pressure estimation using smart phones," *IEEE Trans. Biomed. Eng.*, vol. 60, no. 4, pp. 1080–1089, 2013.

[7] G. Thambiraj, U. Gandhi, U. Mangalanathan, V. Jose, and M. Anand, "Investigation on the effect of womersley number, ECG and PPG features for cuff less blood pressure estimation using machine learning," *Biomed Signal Proces*, vol. 60, p. 101942, 2020.

[8] J. Solà, M. Proença, D. Ferrario, J.-A. Porchet, A. Falhi, O. Grossenbacher, Y. Allemann, S. F. Rimoldi, and C. Sartori, "Noninvasive and nonocclusive blood pressure estimation via a chest sensor," *IEEE Trans. Biomed. Eng.*, vol. 60, no. 12, pp. 3505–3513, 2013.

[9] R. Mukkamala, J.-O. Hahn, and O. T. Inan, "Toward ubiquitous blood pressure monitoring via pulse transit time: Theory and practice," *IEEE Trans. Biomed. Eng.*, vol. 62, no. 8, pp. 1879–1901, 2015.

[10] X.-R. Ding and Y.-T. Zhang, "Continuous cuffless blood pressure estimation using pulse transit time and photoplethysmogram intensity ratio," *IEEE Trans. Biomed. Eng.*, vol. 63, no. 5, pp. 964–972, 2016.

[11] Z. Tang, T. Tamura, and M. Sekine, "A chair–based unobtrusive cuffless blood pressure monitoring system based on pulse arrival time," *IEEE J. Biomed. Health Inform.*, vol. 21, no. 5, pp. 1194–1205, 2017.

[12] M. Kachuee, M. M. Kiani, and H. Mohammadzade, "Cuffless blood pressure estimation algorithms for continuous health-care monitoring," *IEEE Trans. Biomed. Eng.*, vol. 64, no. 4, pp. 859–869, 2017.

[13] K. Sel, J. Zhao, B. Ibrahim, and R. Jafari, "Measurement of chest physiological signals using wirelessly coupled bio-impedance patches," in *2019 41st Annual International Conference of the IEEE Engineering in Medicine and Biology Society (EMBC)*, pp. 376–381, 2019.

[14] B. Ibrahim and R. Jafari, "Cuffless blood pressure monitoring from an array of wrist bio-impedance sensors using subject-specific regression models: Proof of concept," *IEEE Trans. Biomed. Circuits Syst.*, vol. 13, no. 6, pp. 1723–1735, 2019.

[15] T. H. Huynh, R. Jafari, and W.-Y. Chung, "Noninvasive cuffless blood pressure estimation using pulse transit time and impedance plethysmography," *IEEE Trans. Biomed. Eng.*, vol. 66, no. 4, pp. 967–976, 2019.

[16] T. H. Huynh, R. Jafari, and W.-Y. Chung, "An accurate bioimpedance measurement system for blood pressure monitoring," *Sens.*, vol. 18, no. 7, 2018.

[17] T.-W. Wang, W.-X. Chen, H.-W. Chu, and S.-F. Lin, "Single-channel bioimpedance measurement for wearable continuous blood pressure monitoring," *IEEE Trans. Instrum. Meas.*, vol. 70, pp. 1–9, 2021.

[18] B. Ibrahim and R. Jafari, "Cuffless blood pressure monitoring from a wristband with calibration-free algorithms for sensing location based on bio-impedance sensor array and autoencoder," *Scientific reports*, vol. 12, no. 1, p. 319, 2022.

[19] K. Sel, D. Osman, N. Huerta, A. Edgar, R. I. Pettigrew, and R. Jafari, "Continuous cuffless blood pressure monitoring with a wearable ring bioimpedance device," *npj Digital Medicine*, vol. 6, no. 1, p. 59, 2023.

[20] K. Lee and H.-J. Yoo, "Simultaneous electrical bio-impedance plethysmography at different body parts: Continuous and non-invasive monitoring of pulse wave velocity," *IEEE Trans. Biomed. Circuits Syst.*, vol. 15, no. 5, pp. 1027–1038, 2021.

[21] L. D. Montgomery and R. W. Montgomery, "Rheoencephalographic and electroencephalographic measures of cognitive workload: analytical procedures," *Biol Psychol*, vol. 40, no. 1-2, pp. 143–159, 1995.

[22] A. H. Meghdadi, D. Popovic, G. Rupp, S. Smith, and C. Berka, "Transcranial impedance changes during sleep: A rheoencephalography study," *IEEE J. Transl. Eng. Health Med.*, vol. 7, pp. 1–7, 2019.

[23] C. González, E. Jensen, P. Gambús, and M. Vallverdú, "Entropy measures as descriptors to identify apneas in rheoencephalographic signals," *Entropy*, vol. 21, no. 6, 2019.

[24] M. Bodo, M. Simovic, F. Pearce, A. Ahmed, and R. Armonda, "Correlation of rheoencephalogram and intracranial pressure: results of a rat study," *Physiological measurement*, vol. 36, no. 10, p. N115—26, 2015.

[25] C. Robba, S. Bacigaluppi, D. Cardim, J. Donnelly, A. Bertuccio, and M. Czosnyka, "Non-invasive assessment of intracranial pressure," *Acta neurologica Scandinavica*, vol. 134, 10 2015.

[26] M. Bodo, M. Simovic, F. Pearce, A. Ahmed, and R. Armonda, "Correlation of rheoencephalogram and intracranial pressure: results of a rat study," *Physiological Measurement*, vol. 36, pp. N115–N126, sep 2015.

[27] W. Traczewski, M. Moskaa, D. Szwabowska, I. Gociński, and J. Polak, "[the role of computerized rheoencephalography in the assessment of normal pressure hydrocephalus. preliminary report]," *Neurologia i Neurochirurgia Polska*, vol. 39, no. 4, pp. 287–293, 2005.

[28] J. Chen, L. Ke, Q. Du, Y. Zheng, and Y. Liu, "Cerebral blood flow autoregulation measurement via bioimpedance technology," *IEEE Transactions on Instrumentation and Measurement*, vol. 71, pp. 1–8, 2022.

[29] H. Ha, W. Sijbers, R. Van Wegberg, J. Xu, M. Konijnenburg, P. Vis, A. Breeschoten, and S. Song, "A bio-impedance readout IC with digital-assisted baseline cancellation for two-electrode measurement," *IEEE J. Solid-State Circuits*, vol. 54, no. 11, pp. 2969–2979, 2019.

[30] B. Taji, A. D. C. Chan, and S. Shirmohammadi, "Effect of pressure on skin-electrode impedance in wearable biomedical measurement devices," *IEEE Trans. Instrum. Meas.*, vol. 67, no. 8, pp. 1900–1912, 2018.

[31] J. Xu, S. Mitra, C. Van Hoof, and R. F. a. Yazicioglu, "Active electrodes for wearable EEG acquisition: Review and electronics design methodology," *IEEE Rev. Biomed. Eng.*, vol. 10, pp. 187–198, 2017.

[32] A. Savitzky and M. Golay, "Smoothing and differentiation of data by simplified least squares procedures," *Anal. Chem.*, vol. 36, no. 8, pp. 1627–1639, 1964.

[33] M. Panwar, A. Gautam, D. Biswas, and A. Acharyya, "PP-Net: A deep learning framework for PPG-based blood pressure and heart rate estimation," *IEEE Sensors J.*, vol. 20, no. 17, pp. 10000–10011, 2020.

[34] A. Zarei, "Automatic detection of obstructive sleep apnea using wavelet transform and entropy-based features from single-lead ECG signal," *IEEE J. Biomed. Health Inform.*, vol. 23, no. 3, pp. 1011–1021, 2019.

[35] M. Farshad and J. Sadeh, "A novel fault-location method for HVDC transmission lines based on similarity measure of voltage signals," *IEEE Trans. Power Del.*, vol. 28, no. 4, pp. 2483–2490, 2013.

[36] U. M. Khaire and R. Dhanalakshmi, "Stability of feature selection algorithm: A review," *Journal of King Saud University - Computer and Information Sciences*, 2019.

[37] Y. Qi, *Random Forest for Bioinformatics*, pp. 307–323. Boston, MA: Springer US, 2012.

[38] B. Yang, X. Zhu, Y. Liu, and H. Liu, "A single-channel eeg based automatic sleep stage classification method leveraging deep one-dimensional convolutional neural network and hidden markov model," *Biomedical Signal Processing and Control*, vol. 68, p. 102581, 2021.

[39] B. Yang, W. Wu, Y. Liu, and H. Liu, "A novel sleep stage contextual refinement algorithm leveraging conditional random fields," *IEEE Transactions on Instrumentation and Measurement*, vol. 71, pp. 1–13, 2022.

[40] B. Yang and H. Liu, "Automatic identification of insomnia based on single-channel eeg labelled with sleep stage annotations," *IEEE Access*, vol. 8, pp. 104281–104291, 2020.

[41] N. Cristianini and J. Shawe-Taylor, *An Introduction to Support Vector Machines: And Other Kernel-Based Learning Methods*. USA: Cambridge University Press, 1999.

[42] F. Miao, X. Wang, L. Yin, and Y. Li, "A wearable sensor for arterial stiffness monitoring based on machine learning algorithms," *IEEE Sensors J.*, vol. 19, no. 4, pp. 1426–1434, 2019.

[43] J. Shukla, M. Barreda-Angeles, J. Oliver, G. C. Nandi, and D. Puig, "Feature extraction and selection for emotion recognition from electrodermal activity," *IEEE Transactions on Affective Computing*, vol. 12, no. 4, pp. 857–869, 2019.

[44] D. Liu, H. Qian, G. Dai, and Z. Zhang, "An iterative svm approach to feature selection and classification in high-dimensional datasets," *Pattern Recognition*, vol. 46, no. 9, pp. 2531–2537, 2013.

[45] J.-Y. Wang, T. Healey, A. Barker, B. Brown, C. Monk, and D. Anumba, "Magnetic induction spectroscopy (mis)—probe design for cervical tissue measurements," *Physiological measurement*, vol. 38, no. 5, p. 729, 2017.

[46] Z. Liao, S. Jin, A. Kuwahata, M. Sekino, and H. Tabata, "Coherent detection stochastic resonance assisted biomagnetometer for measuring magnetocardiography at room temperature," *Applied Physics Express*, vol. 14, no. 9, p. 097001, 2021.